International Journal of Modern Physics C, Vol. 11, No. 0 (2000) 000–000

TUMBLING MOTION OF ELLIPTICAL PARTICLES IN VISCOUS TWO-DIMENSIONAL FLUIDS

GERALD H. RISTOW
Fachrichtung Theoretische Physik, Universität des Saarlandes
Postfach 15 11 50, 66041 Saarbrücken, Germany

Received (February 24, 2000)
Revised (April 20, 2000)

The settling dynamics of spherical and elliptical particles in a viscous Newtonian fluid are investigated numerically using a finite difference technique. The terminal velocity for spherical particles is calculated for different system sizes and the extrapolated value for an infinite system size is compared to the Oseen approximation. Special attention is given to the settling and tumbling motion of elliptical particles where their terminal velocity is compared with the one of the surface equivalent spherical particle.

1. Introduction

Computational fluid dynamics is a very fascinating and still rather challenging field of study. This is especially true when solid particles are immersed in a viscous fluid leading to a two-phase flow problem which can be dealt with in two fashions: (a) Through a continuum approach involving both phases simultaneously or (b) by solving the governing equations separately for each phase and combining the results appropriately.

In this article, we will use the latter approach and study the sinking and tumbling motion of spherical and elliptical particles in two-dimensional spatially bound viscous fluids. The fluid motion is solved on an equally-spaced finite difference grid and the particle-fluid interaction is taken into account by (a) treating the particle as an additional moving boundary and (b) by integrating the stress tensor over the surface of the particle in order to calculate the force and torque on the particle. The details of the algorithm are outlined in Sect. 2. The results of our numerical scheme are validated in Sect. 3 by comparing them with the Oseen approximation in the low Reynolds number limit. In Sect. 4, the settling and tumbling dynamics of elliptical particles are studied for different aspect ratios and system sizes. Special focus is given to the magnitude and the decay of the oscillations in the tumbling motion of the ellipses. Our results are summarized in Sect. 5.

2. Numerical Modeling

A finite difference technique is used to study the sinking dynamics of spherical and elliptical particles in two-dimensional, bounded domains filled with a viscous fluid.

2.1. *Governing equations*

Since the obtained velocities are well-below the speed of sound, the fluid can be treated as incompressible, i.e. having a constant density ρ_f. The fluid velocity $\vec{v}$ and the pressure p are measured in a fixed laboratory system and the governing equations are the Navier-Stokes equations which read in dimensionless form

$$\frac{\partial \vec{v}}{\partial t} + (\vec{v} \cdot \nabla)\vec{v} = -\nabla p + \frac{1}{\mathrm{Re}} \nabla^2 \vec{v} + f \ , \tag{1}$$

where Re denoted the Reynolds number and f an external force, e.g. gravity g.

The only parameter that describes the physical situation is the dimensionless Reynolds number Re. Given a characteristic velocity U, a characteristic length D, e.g. the particle diameter, and the viscosity of the fluid $\nu := \eta/\rho_f$ its definition is

$$\mathrm{Re} := \frac{U\,D}{\nu} \ . \tag{2}$$

For an incompressible fluid the continuity equation

$$\frac{\partial \rho_f}{\partial t} + \nabla \cdot (\rho_f \vec{v}) = 0 \tag{3}$$

reduces to

$$\nabla \cdot \vec{v} = 0 \ . \tag{4}$$

We study the motion of rigid particles in fluids by introducing the particles as additional, moving boundaries.[1] The force acting on the particle by the fluid is calculated via integration of the stress tensor σ along the particle's circumference,[2]

$$\vec{F}_s = \int_{\text{circumference}} \sigma \cdot \vec{S}\, dA \ , \tag{5}$$

where $\vec{S}$ stands for the outward-pointing surface normal along the circumference and

$$\sigma = -p\, I + \eta \left(\nabla \vec{v} + (\nabla \vec{v})^t \right) \tag{6}$$

using a matrix notation with I being the unity matrix and η the fluid viscosity. Instead of integrating Eq. (5) directly along the particle circumference as proposed by our algorithm, an analytic expansion for the fluid field can also be used which is not as straight forward and more demanding on the computer resources.[3]

When Eqs. (1) are discretized in time first, $t = t_0 + n\Delta t$, the general form reads [4]

$$\begin{aligned} \frac{\vec{v}^{n+1} - \vec{v}^{n}}{\Delta t} \quad &+ \quad \theta \left[(\vec{v}^{n+1} \nabla) \vec{v}^{n+1} - \frac{1}{\mathrm{Re}} \nabla^2 \vec{v}^{n+1} - \vec{f}^{n+1} \right] \\ &+ \quad (1-\theta) \left[(\vec{v}^{n} \nabla) \vec{v}^{n} - \frac{1}{\mathrm{Re}} \nabla^2 \vec{v}^{n} - \vec{f}^{n} \right] + \nabla p^{n+\tau} = 0 \ , \end{aligned} \tag{7}$$

where the parameter θ fulfills $0 < \theta < 1$. For $\theta = 0$ we end up with an *explicit* scheme and for $\theta = 1$ we get a *fully implicit* scheme. A very efficient method results for $\theta = \frac{1}{2}$ called the *Crank-Nicolson Scheme* which we will use to investigate the dynamics of the fluid. The parameter τ is set to the value that will give the lowest truncation error for the desired algorithm.

One writes the Navier-Stokes equations and the continuity equation in the new variables v_x^{n+1}, v_y^{n+1} and $p^{n+\tau}$ and ends up with a nonlinear algebraic system for the unknowns

$$\begin{aligned} L_x(v_x^{n+1}, v_y^{n+1}, p^{n+\tau}) &= 0 \\ L_y(v_x^{n+1}, v_y^{n+1}, p^{n+\tau}) &= 0 \\ D(v_x^{n+1}, v_y^{n+1}) &= 0 \;. \end{aligned} \tag{8}$$

This system is solved by an iterative procedure where m denotes the iteration index

$$\begin{aligned} v_x^{m+1} - v_x^m + \kappa L_x(v_x^{n+1}, v_y^{n+1}, p^{n+\tau}) &= 0 \\ v_y^{m+1} - v_y^m + \kappa L_y(v_x^{n+1}, v_y^{n+1}, p^{n+\tau}) &= 0 \\ p^{m+1} - p^m + \lambda D(v_x^{n+1}, v_y^{n+1}) &= 0 \;, \end{aligned} \tag{9}$$

and the parameters κ and λ are chosen in such a way that convergence of this scheme is guaranteed.

From a linear stability analysis one obtains as necessary condition for convergence of the procedure given by Eqs. (9) the condition

$$\frac{\kappa}{\Delta x^2}\left(\frac{4\theta}{\mathrm{Re}} + \frac{\Delta x^2}{2\Delta t} + 2\lambda\right) \leq 1 \;,\; \kappa > 0, \lambda > 0 \;. \tag{10}$$

It can be obtained in the same way as for the artificial compressibility method.[4]

For given values of Δt, Δx and κ Eq. (10) gives an upper bound for the iteration parameter λ

$$\lambda < \lambda_{\mathrm{max}} := \frac{\Delta x^2}{2\kappa} - \left(\frac{2\theta}{\mathrm{Re}} + \frac{\Delta x^2}{4\Delta t}\right) \;. \tag{11}$$

For each iteration it is crucial for a fast convergence of the iterative algorithm that optimal values for the parameters κ and λ are used. Peyret and Taylor [4] pointed out that the best value of λ is close but not equal to λ_{max} and the simulations for our system confirmed this. But the rule of thumb that κ_{opt} should be of the order of Δx^2 was only true in our case when the particle was fixed in space. When the particle was allowed to move according to the calculated force no easy scaling law could be found since the value depends on Δx, Δt and η. In this case, the optimum values for the parameters were determined by a few test runs.[1]

The convergence rate of our algorithm is illustrated by studying the sinking dynamics of a cylinder with a radius of 1.5 cm under gravity using $g = 981\,\mathrm{cm/s}^2$ released in a two-dimensional box with dimensions 10x20 cm. The particle is 10% denser than the fluid and the fluid viscosity was set to 100 times the value of

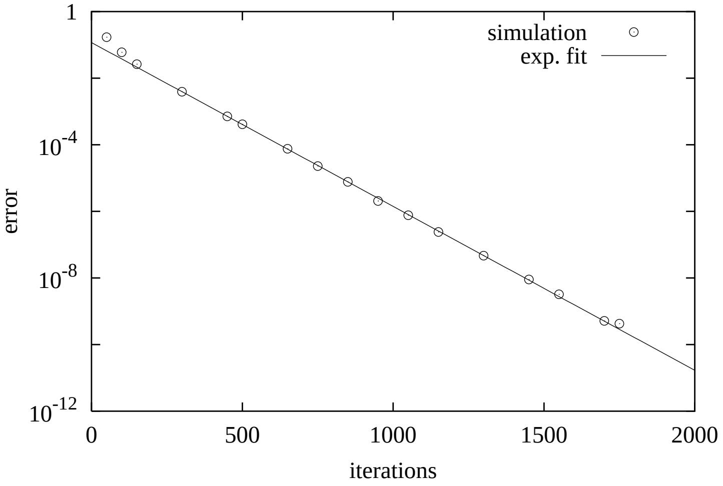

Fig. 1. Accuracy in the calculation of the velocity field as function of the number of iterations, measured via the divergence of the velocity. The solid line corresponds to an exponential fit with an exponent of -1.

water. First, we show in Fig. 1 the number of iterations needed by our algorithm to calculate the velocity field up to a desired accuracy for a grid size of 64x128 equally-spaced points. The solid line corresponds to an exponential fit with an exponent of -1 and one reads off that the accuracy increases by one order of magnitude every 200 iterations.

For iterative algorithms, the number of iterations to obtain a desired accuracy usually increases with the number of unknowns, here grid points. This dependence is shown in Fig. 2 for our algorithm using the same system parameters as described above and an accuracy of 10^{-7}. The number of iterations increases with the number of grid points, as expected, and the data points corresponding to more than 2000 grid points could be well-described by a power-law fit with an exponent of 0.72. Please note that the total runtime of the algorithm will exhibit a scaling relation with an exponent of 1.72 since the time required for one iteration usually increases linearly with the number of unknowns.

2.2. *Spherical particles*

As noted earlier, the motion of the rigid particles is treated as an additional, moving boundary. A straight-forward approach to obtain the pressure term on the staggered grid is sketched in Fig. 3a, where the shape of the particle is approximated by boxes (or squares if the grid spacing is the same in both coordinate directions) and the force on the particle is calculated by summing over the outer edges of the boxes along the Cartesian coordinate directions. The two directions decouple when one first sums along the horizontal and later along the vertical lines, indicated by the two arrows in the upper left corner. Since the fluid pressure is not well-defined inside a

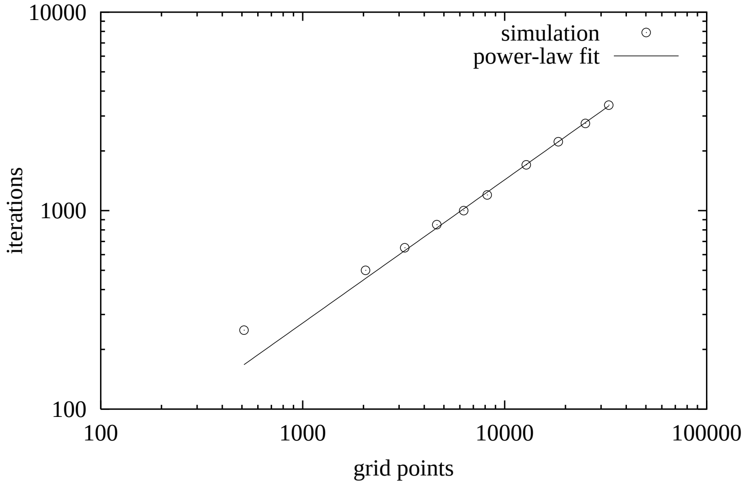

Fig. 2. Number of iterations for a desired accuracy as function of the number of grid points. The solid line corresponds to a power-law fit with an exponent of 0.72.

rigid particle, only points *outside* the particle are used for calculating the pressure. This makes the particle appear *larger* than it really is, shown as gray-shaded area in Fig. 3a. Consequently, the calculated force is usually over-estimated but approaches the theoretical value as the grid spacing decreases. This is shown in Fig. 3b for a cylinder at rest with a diameter of 2 cm in a box of 20x40 cm. The theoretical value for the buoyancy force per unit length is $F_s = -3.1\,\mathrm{g/s}^2$ which is reached within a 5% error for a spacing of 0.1 which corresponds to more than 100 grid points in the x-direction and roughly 10 points across the particle diameter. Also shown as solid line in Fig. 3b is a parabolic fit to the data points which illustrates the approach to the theoretical value with decreasing grid spacing. The velocity gradients needed in Eq. (6) to complete the calculation of the force on the particle are calculated by choosing the appropriated grid points from the staggered MAC grid around the grid points that entered the pressure calculation.[4] A somewhat similar approach was used in a multi-particle simulation to study the dynamics of suspensions.[5]

The above-described algorithm for calculating the force exerted by the fluid on the particle has two drawbacks: (i) Large fluctuations are obtained when the grid spacing is changed, see Fig. 3b, and (ii) the corresponding particle size, shown in gray in Fig. 3a, does not match the physical size of the particle but it is mostly over-estimated by the numerical algorithm.

To overcome these problems, a two-step procedure was used. Realizing that the only contribution to the stress tensor in Eq. (6) for a particle at rest comes from the pressure p, correcting these contributions seemed favorable. First, the pressure is linearly extrapolated to the *real* particle surface, indicated in Fig. 4a by $\star$, thus making the errors in the particle size much smaller. Second, instead of working with rectangular blocks which decouple the x- and y-components of

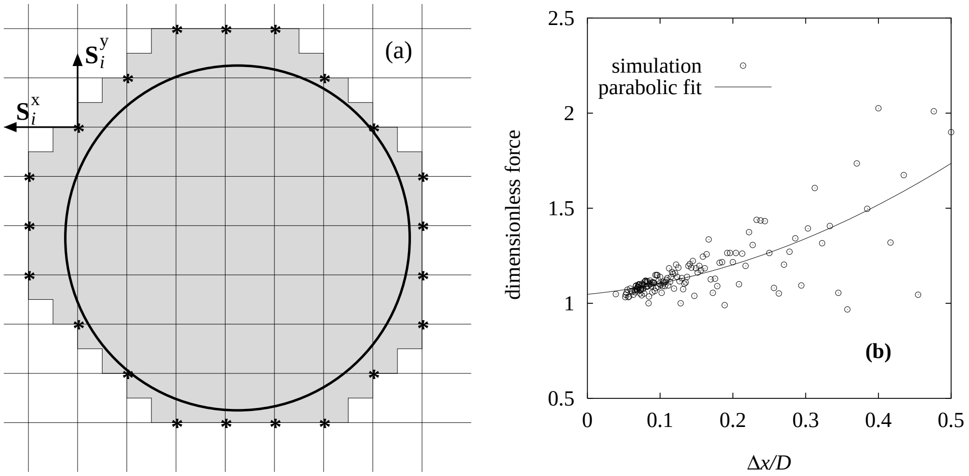

Fig. 3. Straight-forward approach to calculate the force on a particle: (a) Pressure points, denoted by $\star$, used in the calculation and (b) force on the cylinder as function of the dimensionless grid spacing. The gray-shaded area illustrates the grid-dependence of the *real* particle size and the two decoupled surface normals are also shown in the upper left corner.

the force contributions, the force calculation at each sample point uses the *actual* surface normal, which is indicated by $\mathbf{S}_i$ in Fig. 4a. All surface points are kept in a list ordered by their arc length (angle). The length of the surface element at each sample point then uses the averaged arc length to their left and right neighbor points. This procedure *always* leads to a particle size which matches the physical size exactly in the case when a spherical cylinder is used. The force fluctuations do no longer show a systematic dependence on the grid spacing, which is shown in Fig. 4b for the same parameters as were used to generate Fig. 3b. Also note that the magnitude of the fluctuations is far less for the improved force calculation, allowing for a twice as large grid spacing in order to obtain the same accuracy as before. The extrapolated force for an infinitely dense grid also gives a more accurate value than the old procedure outlines above.

2.3. *Elliptical particles*

As long as spherical cylinders move close to the centerline of the container, particle rotations can be neglected. This is no longer true if the particle motion takes place close to one of the side boundaries or if deviations from the spherical particle shape are considered, e.g. elliptical shapes as sketched in Fig. 5a. The torque on a particle must then be calculated and is given by,

$$\vec{\tau}_s = \int_{\text{circumference}} \vec{R}^s \times (\sigma \cdot \vec{S})\, dA \ , \tag{12}$$

where $\vec{R}^s$ denotes the vector from the center of mass of the particle to the surface element under consideration.

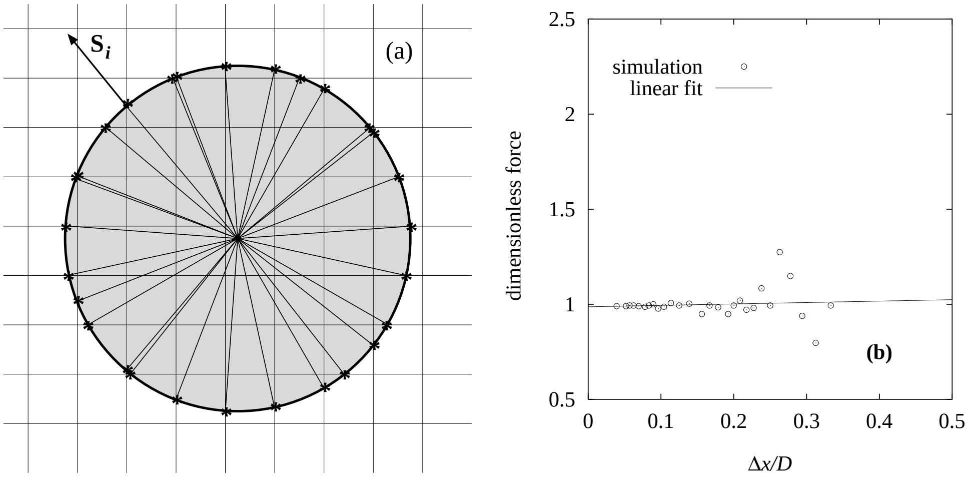

Fig. 4. Improved approach to calculate the force on a particle: (a) Pressure points, denoted by ⋆, used in the calculation and (b) force on the cylinder as function of the dimensionless grid spacing. In contrast to Fig. 3a, now the *exact* particle size is used for all grid spacings and the surface normal usually has components along both spatial directions, shown in the upper left corner.

Even though the force (and torque) on an elliptical particle can be calculated in a similar fashion as described in the preceding section for spherical particles, two additional problems arise. First, no simple analytic expression for the arc length between two arbitrary surface points is known and second, the surface normal ($\vec{S}$) has to be calculated separately for each sampling point since it is not parallel to the vector from the center of mass to the surface element ($\vec{R}^s$), as shown in Fig. 5a in the upper left corner.

The latter point was addressed by calculating the surface normal analytically in the reference frame of the ellipse and by rotating it back to the laboratory frame. For the calculation of the arc length, a simple linear interpolation to the two neighboring points was used. Since ellipses are concave objects, this approach will always slightly *underestimate* the surface area of the ellipse, and we introduced an intermediate point in each direction in order to reduce this error. The accuracy of this approach is demonstrated in Fig. 5b, where we plot the force on an ellipse having an aspect ratio of 2.25 as function of the dimensionless grid spacing. The ellipse has the same surface area as the circle used to calculate the points shown in Fig. 4b above, thus showing the same initial vertical force contribution due to gravity. The accuracy of the two results is comparable and is far better than the original algorithm presented in Fig. 3. The extrapolated force for an infinitely dense grid is hardly distinguishable from the theoretical value. Thus the presented force calculation for an elliptical particle can be regarded as being as accurate as for a spherical particle.

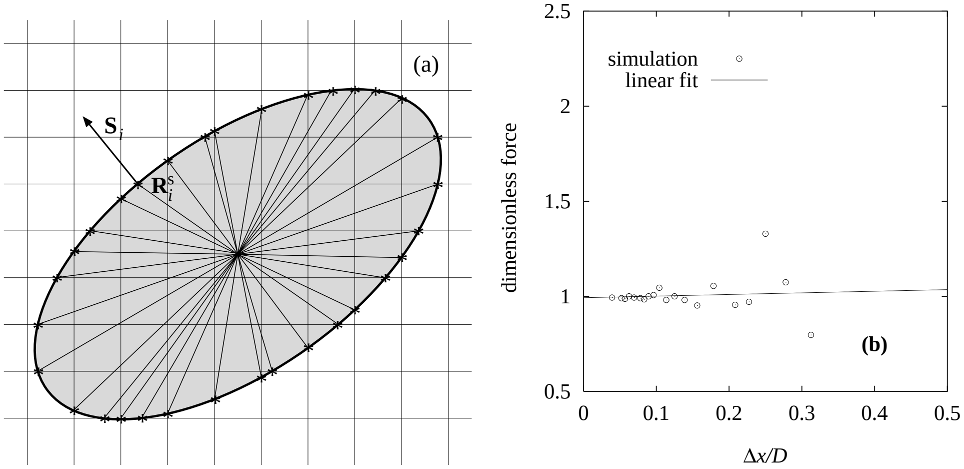

Fig. 5. Calculating the force on an elliptical particle: (a) Pressure points, denoted by $\star$, used in the calculation and (b) force on the ellipse as function of the dimensionless grid spacing.

3. Program Validation

In the preceding paragraphs, we showed that the improved algorithm gives accurate results for the force exerted on a spherical or elliptical cylinder at rest, see Figs. 4 and 5, respectively. We now turn our attention to a moving particle and demonstrate that the terminal velocity of a cylinder in a viscous fluid as calculated by the above described algorithm agrees with the theoretical value in the low Reynolds number limit. In this limit, the Oseen approximation leads to an analytic expression for the viscous drag force per unit length of the cylinder.[6,7] This can be used to derive an *implicit* expression for the terminal velocity of a cylinder, V_c, which reads

$$\frac{V_c}{\ln(4\nu/(RV_c))+0.5} = \frac{\rho_c-\rho_f}{4\eta} gR^2 \ . \tag{13}$$

Here ρ_c stands for the density of the cylinder, R denotes its radius and $\nu \equiv \frac{\eta}{\rho_f}$. No analytic expression exists for arbitrary Reynolds numbers. After the particle is released from rest, the calculated force and torque exerted by the fluid on the particle is used to calculate the particle position, orientation, velocity and angular velocity via the Verlet algorithm. In the iterations for the fluid field for the next time step, the particle is treated as an additional moving boundary by giving all velocity points covered by the particle a value which corresponds to a rigid particle.

The approximation from Eq. (13) is only valid for an infinite system and we have to extrapolate the numerically obtained terminal velocities of the cylinder correspondingly.[8] The procedure we used is illustrated in Fig. 6a for a fluid viscosity of $\eta = 5\,\mathrm{g/(cm\,s)}$ and the two cylinder radii 1.0 and 0.8 cm, respectively. The density contrast was chosen again as 10%, see Sect. 2.1. The terminal velocity is plotted as a function of the dimensionless parameter D/L where $D \equiv 2R$ stands for the

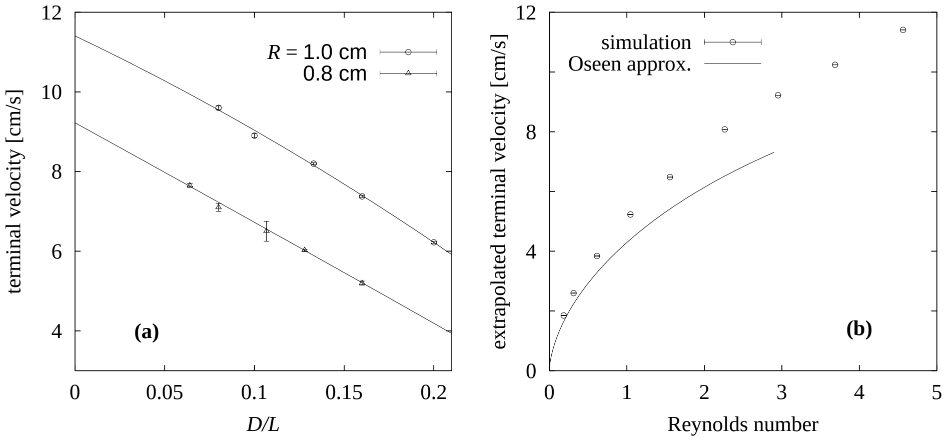

Fig. 6. Terminal velocity of cylinders: (a) As function of the diameter to system size ratio D/L where the solid lines are quadratic fits to the data points and (b) extrapolated value as function of the Reynolds number. Also shown as solid line is the Oseen approximation.

cylinder diameter and L for the system width. A quadratic fit is used to obtain the extrapolated terminal velocities for an infinite system, i.e. in our case the value at the intersection with the ordinate.

The terminal velocities obtained in this fashion are plotted in Fig. 6b as a function of the Reynolds number Re. The error bars stem from the fitting algorithm. Also shown as solid line is the Oseen approximation, Eq. (13). Since the approximation is only valid for low Reynolds numbers, it is not surprising that the agreement between the numerical results and the analytic expression becomes better and better the smaller the Reynolds number gets. However, the smaller the particle becomes the more grid points are needed to avoid unphysical oscillations in the particle velocity. This only made calculations down to a cylinder radius of 0.25 cm feasible due to the limitations in computer memory and CPU time. Please note that for $R = 0.25$ cm the corresponding Reynolds number is still moderate (Re≈ 0.14) thus making a value difference of less than 24% in Fig. 6b for the left-most data point ($R = 0.25$ cm) more than acceptable.

4. Motion of Elliptical Particles

When elliptical particles are considered, the particle orientation is important and particle rotation has to be taken into account as well. In the creeping flow regime, the particle orientation will in principle not change during the settling process but the settling velocity depends significantly on the orientation of the major axis with respect to the container bottom (horizontal direction).[9]

If the *major* axis is parallel to gravity, the resistance will be lowest and the terminal velocity highest. However, such a particle orientation seems to be unstable for moderate Reynolds numbers where the ellipse prefers to sink with the lowest

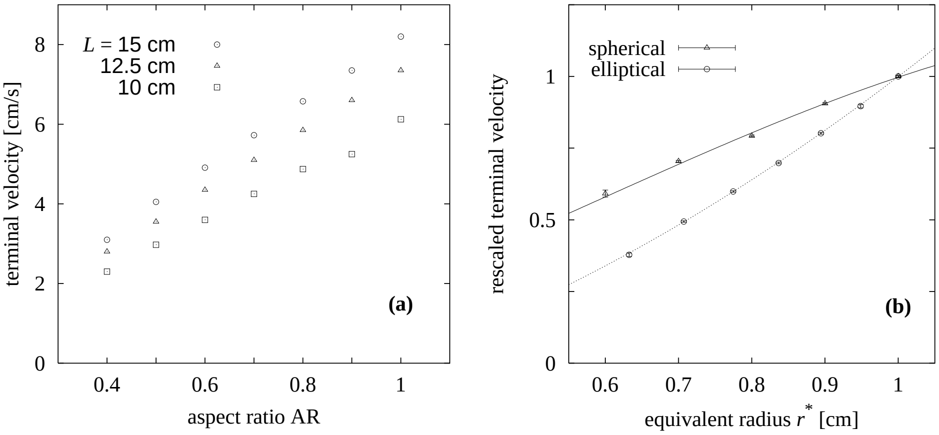

Fig. 7. Terminal velocity of ellipses: (a) As function of the aspect ratio and (b) as function of the corresponding equivalent cylinder with a spherical cross-section $d = 2r^*$ and for a system size of $L = 15\,\text{cm}$. For comparison, we shown in (b) also the values for a spherical particle and two polynomial fits to guide the eye. The error bars are roughly of the order of the symbol size.

possible velocity, thus aligning the *minor* axis parallel to gravity.[10,11]

4.1. *Terminal Velocity*

For the simulation parameters used in this article, we also found that elliptical particles tend to align their minor axis with gravity in the long run. In order to avoid long transition periods, we therefore start the elliptical particle with an angle of the major axis with the horizontal of 0° to determine the terminal velocity for different aspect ratios $\text{AR} = a/b$ where a and b denote the minor and major axis of the elliptical cross-section, respectively. In Fig. 7a, the dependence of the terminal velocity on the aspect ratio is shown for three different system sizes L. As in the case for a spherical particle, see Fig. 6a, the velocity increases with increasing system size since the drag force due to the back-flowing fluid decreases.

The surface area of the cross-section of the elliptical particle is given by

$$F_e = \pi a\, b$$

whereas the surface area of a spherical particle with radius r is given by

$$F_s = \pi r^2 \ .$$

In order to compare the dynamics of elliptical and spherical particles, one defines a surface equivalent spherical particle for the ellipse with radius

$$r^* = \sqrt{a\, b}$$

which has the same surface area as the elliptical particle.

This comparison is shown in Fig. 7b for a system size of $L = 15\,\mathrm{cm}$ and a viscosity of $\eta = 5\,\mathrm{g/(cm\ s)}$. The data points were approximated by polynomial fits to guide the eye. The terminal velocity for spherical cylinders is always *higher* than the one for elliptical particles when the surface equivalent spherical cylinder with radius r^* is considered. Due to the fact that the broad side of the ellipse is always turned into the stream, the terminal velocity is nearly reduced by 50% for a value of $r^* = 0.55\,\mathrm{cm}$ ($b = 1\,\mathrm{cm}$). The terminal velocities for the spherical and elliptical cross-section shown in Fig. 7b were rescaled by the value for the unit spherical cross-section.

4.2. *Tumbling Motion*

If an elliptical particle is released in a finite container filled with a viscous fluid under gravity, the particle will for high enough Reynolds numbers in general undergo a tumbling motion until its minor axis is perfectly aligned with the direction of gravity and a translational motion until it sinks in the middle of the container.[12] The latter is given by the symmetry of the problem and is also true for spherical cylinders.[13] Numerical simulations indicate that below a critical Reynolds number, an elliptical particle will turn vertical in a Newtonian fluid.[14] However, in our numerical simulations we did not find such a behavior which might be due to the different simulation parameters.

To illustrate this point, we show in Figs. 8a,b the settling motion of two elliptical particles in a container of size 10x40 cm having an aspect ratio of 0.9 and 0.6, respectively. Both particles were initially released at an angle of $\pi/4$ (45°) and the tumbling motion is clearly visible in both cases but being more pronounced for lower aspect ratios (e.g. Fig. 8b). Also note the translational motion which drags the particle towards the centerline of the container.

For the particle motion depicted in Fig. 8b, the settling and tumbling dynamics are quantified by showing the settling velocity as function of time in Fig. 8c and the particle orientation, minor axis with respect to gravity, as function of time in Fig. 8d. The latter graph shows how the oscillations in the orientation decrease in time and how they overshoot the value of zero after around 2 s after the particle was released. This overshooting seems to be more pronounced and the decay seems to be less pronounced when the aspect ratio is decreased from 0.9 to 0.7. However, the opposite tendency is observed upon decreasing the aspect ratio even further down to 0.6 which is due to the fact that the particle comes closer to the rigid vertical side walls. It would be interesting to better quantify how the oscillations decay as function of aspect ratio and container width where investigations are underway.

The settling velocity as function of time for an elliptical particle with an aspect ratio of 0.6 is shown in Fig. 8c. In the long run, the velocity approaches the terminal velocity of $-3.65\,\mathrm{cm/s}$ which was added to the figure as dashed line. Since the initial particle orientation was $\pi/4$, the particle first moves to the left. During this motion, the angle decreases and when it passes through zero, a force component to the right, towards the center of the container, sets in. Please note how the particle orientation

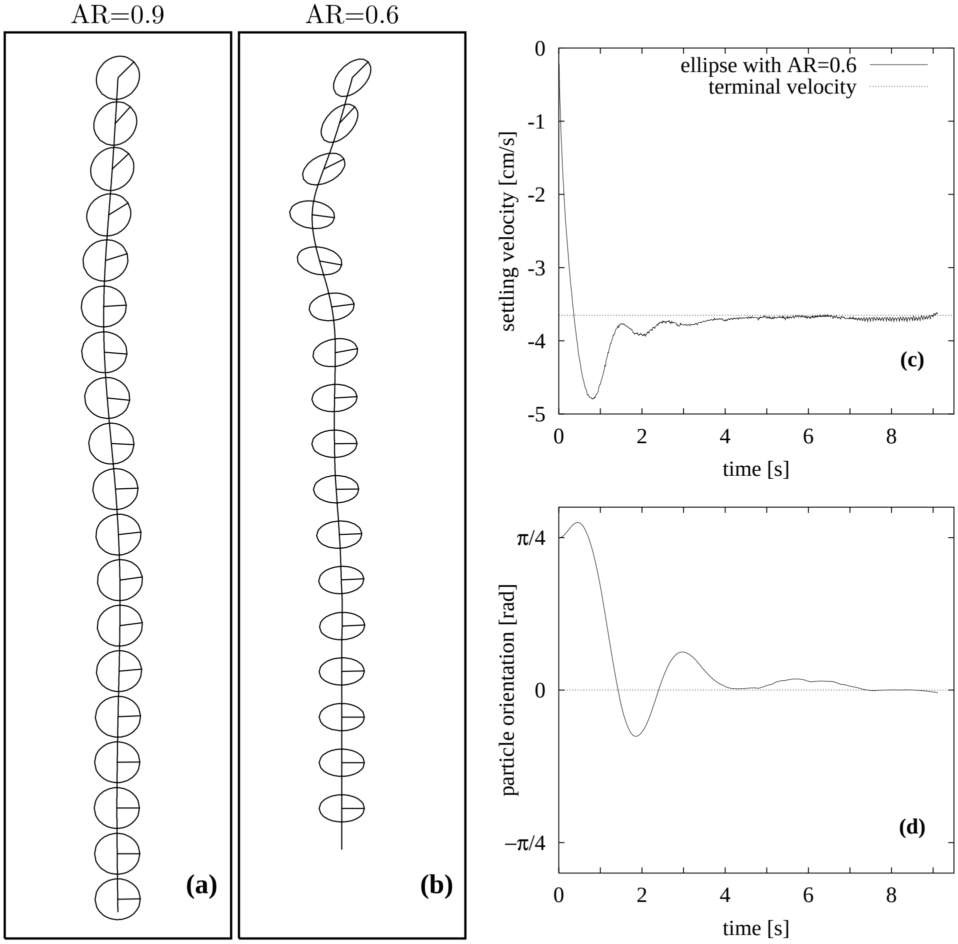

Fig. 8. Settling dynamics of elliptical particles having an aspect ratio of 0.9 (a) and 0.6 (b). For the latter case the settling velocity as function of time is shown in (c) and the particle orientation as function of time in (d). Please note the correlations between the orientation and the velocity.

and the settling velocity are related leading to velocity maxima shortly after the particle orientation deviates the most from zero, i.e. comes the closest in turning the thin side into the stream.

5. Conclusions

We presented an efficient numerical algorithm to study the motion of spherical and elliptical particles in two-dimensional viscous fluids. We validated our algorithm by comparing its results with analytic expressions for fixed and moving particles. in the latter case, good agreement with the Oseen approximation is found in the low Reynolds number limit. However, our algorithm is not restricted to this limit since it solves the full Navier-Stokes equations and can easily be extended to deal with more than one particle.

This procedure was then used to study the settling and tumbling motion of elliptical particles. The terminal velocity was compared to the one of the surface equivalent sphere where we found that the terminal velocity is drastically decreased due to the fact that the broad side of the ellipse is always turned into the stream. It was also found that the magnitude and the decay of the tumbling motion depends on the aspect ratio of the ellipse and the container width.

Acknowledgements

Stimulating and very helpful discussions with N. Lu are greatfully acknowledged.

References

1. G. H. Ristow, "Particles Moving in Spatially Bounded, Viscous Fluids," Comput. Phys. Commun. **99,** 43–52 (1996).
2. R. H. Davis, In *Mobile Particulate Systems*, E. Guazzelli and L. Oger, eds., pp. 39–56 (Kluwer, Dordrecht, 1995).
3. W. Kalthoff, S. Schwarzer, and H. J. Herrmann, "Algorithm for the Simulation of Particle Suspensions with Inertia Effects," Phys. Rev. E **56,** 2234–2242 (1997).
4. R. Peyret and T. D. Taylor, *Computational Method for Fluid Flow* (Springer, Heidelberg, 1985).
5. B. Wachmann and S. Schwarzer, "Three-Dimensional Massively Parallel Computing of Suspensions," Int. J. Mod. Phys. C **9,** 759–775 (1998).
6. H. Lamb, *Hydrodynamics* (Cambridge, Cambridge, 1997).
7. E. Guyon, J.-P. Hulin, and L. Petit, *Hydrodynamik* (Vieweg, Braunschweig, 1997).
8. G. H. Ristow, "Wall Correction Factor for Sinking Cylinders in Fluids," Phys. Rev. E **55,** 2808–2813 (1997).
9. R. Clift, J. R. Grace, and M. E. Weber, *Bubbles, Drops, and Particles* (Academic, New York, 1978).
10. R. G. Cox, "The Steady Motion of a Particle of Arbitrary Shape at Small Reynolds Numbers," J. Fluid Mech. **23,** 625–643 (1965).
11. P. Y. Huang, J. Feng, and D. D. Joseph, "The Turning Couples on an Elliptic Particle Settling in a Vertical Channel," J. Fluid Mech. **271,** 1–16 (1994).
12. J. Feng, H. H. Hu, and D. D. Joseph, "Direct Simulation of Initial Value Problems for the Motion of Solid Bodies in a Newtonian Fluid. Part 1. Sedimentation," J. Fluid Mech. **261,** 95–134 (1994).
13. H. H. Hu, D. D. Joseph, and M. J. Crochet, "Direct Simulation of Fluid Particle Motions," Theoret. Comput. Fluid Dynamics **3,** 285–306 (1992).
14. P. Y. Huang, H. H. Hu, and D. D. Joseph, "Direct Simulation of the Sedimention of Elliptic Particles in Oldroyd-B Fluids," J. Fluid Mech. **362,** 297–325 (1998).